Transcutaneous monitoring of hemoglobin derivatives during methemoglobinemia in rats using spectral diffuse reflectance

Transcutaneous monitoring of hemoglobin derivatives during methemoglobinemia in rats using spectral diffuse reflectance

Fahima Khatun,[a,b] Yoshihisa Aizu[c], and Izumi Nishidate[a,*]

[a]Tokyo University of Agriculture and Technology, Graduate School of Bio-Applications and Systems Engineering, Tokyo, Japan

[b]Bangabandhu Sheikh Mujibur Rahman Agricultural University, Faculty of Veterinary Medicine and Animal Science, Department of Pathobiology, Gazipur, Dhaka, Bangladesh

[c]Muroran Institute of Technology, College of Design and Manufacturing Technology, Hokkaido, Japan

Abstract

Significance: Untreated methemoglobinemia may cause severe hypoxemia and even death when methemoglobin levels in the blood stream exceed 70%. Although CO-oximetry can be used to monitor the response to treatment for methemoglobinemia, it is costly and requires an invasive procedure for collecting blood samples from patients. A pulse CO-oximeter with a contact probe can be used to continuously and non-invasively measure the percentage of methemoglobin, as well as the percutaneous oxygen saturation. In terms of the prevention of infectious diseases, however, it is desirable to monitor methemoglobin and oxygen saturation levels in a non-contact manner. Diffuse reflectance spectral imaging is promising as a non-contact, non-invasive, and cost-effective clinical diagnostic tool for methemoglobinemia.

Aim: To demonstrate the feasibility of visible spectral diffuse reflectance for *in vivo* monitoring of hemoglobin derivatives and evaluating methemoglobin production and reduction as well as hypoxemia during methemoglobinemia in rats.

Approach: A new imaging approach based on the multiple regression analysis aided by Monte Carlo simulations for light transport was developed to quantify methemoglobin, oxygenated hemoglobin, and deoxygenated hemoglobin using a hyperspectral imaging system. An *in vivo* experiment with rats exposed to sodium nitrite ($NaNO_2$) at different doses was performed to confirm the feasibility of the method for evaluating the dynamics of methemoglobin, oxygenated hemoglobin, and deoxygenated hemoglobin during methemoglobinemia. Systemic physiological parameters, including the percutaneous arterial oxygen saturation, heart rate (HR), and pulse distention, were measured by a commercially available pulse oximeter, and the results were compared to those obtained by the proposed method.

Results: Both the methemoglobin concentration and methemoglobin saturation rapidly increased with a half-maximum time of <20 min. They reached their maximal values nearly 60 min after the administration of $NaNO_2$. Tissue oxygen saturation dramatically dropped to a minimum of $33.7\% \pm 0.4\%$, $23.1\% \pm 5.6\%$, $8.8\% \pm 1.7\%$, and $9.7\% \pm 5.1\%$ on average for $NaNO_2$ doses of 25, 37.5, 50, and 75 mg/kg, respectively. Changes in methemoglobin concentration and tissue oxygen saturation are indicative of the temporary production of methemoglobin and severe hypoxemia during methemoglobinemia. Profound increases in the HR and pulse distention implied an elevated cardiac output caused by tachycardia and the resultant increase in peripheral blood volume to compensate for the hypoxia and hypoxemia during methemoglobinemia. This was in agreement with the time course of the peripheral hemoglobin volume concentration obtained by the proposed method.

Conclusions: The proposed method is capable of the *in vivo* non-contact simultaneous evaluation of methemoglobin levels and hypoxemia during methemoglobinemia, and that it has potential as a tool for the diagnosis and management of methemoglobinemia.

---

*Address all correspondence to Izumi Nishidate, inishi@cc.tuat.ac.jp

1 Introduction

The spectral features of human skin are often affected by various skin diseases, which cause altered attenuation of light within multiple layers of the skin. In the epidermis and dermis, similar changes are associated with fluctuations in the concentration of melanin and blood-borne pigments, such as hemoglobin.[1] Each chromophore has its own characteristic absorption spectrum in the visible to near-infrared wavelength regions, which change with wavelength and can function as a fingerprint for that molecule. The binding of other molecules to the functional chromophore causes variations in the structure of a molecule, resulting in an altered absorption spectrum for each derivative of a molecule that is formed. Figure 1 shows the extinction coefficient spectra of typical hemoglobin derivatives and melanin at visible wavelengths between 500 and 700 nm.[2–4] The actual absorption spectra of hemoglobin depend primarily upon whether or not the blood is oxygenated, and there are thus two main derivatives, i.e., oxyhemoglobin in oxygenate blood and deoxyhemoglobin in deoxygenated blood. There are also hemoglobin derivatives that are incapable of transporting oxygen molecules, and they are, therefore, collectively known as dyshemoglobins; these include methemoglobin, carboxyhemoglobin, and sulfhemoglobin. The absorption can differ drastically between dysfunctional hemoglobin and functional hemoglobin.[5,6]

Methemoglobin is a dysfunctional form of hemoglobin, in which the ferrous (Fe^{2+}) irons of heme are oxidized to the ferric (Fe^{3+}) state and cannot bind oxygen molecules. Therefore, methemoglobin is incapable of transporting oxygen molecules to peripheral tissues.[7] As a consequence, a large amount of methemoglobin causes methemoglobinemia, which leads to tissue hypoxia.[8] Under normal physiological states, only a small amount (<2%) of hemoglobin exists in the form of methemoglobin.[6] However, a higher percentage is found in individuals who suffer from methemoglobinemia due to genetic diseases[9–12] or exposure to certain chemicals and drugs.[13–17] Severe untreated methemoglobinemia is life-threatening and may cause death when methemoglobin levels in the blood stream exceed 70%.[6,18] There are many case reports of

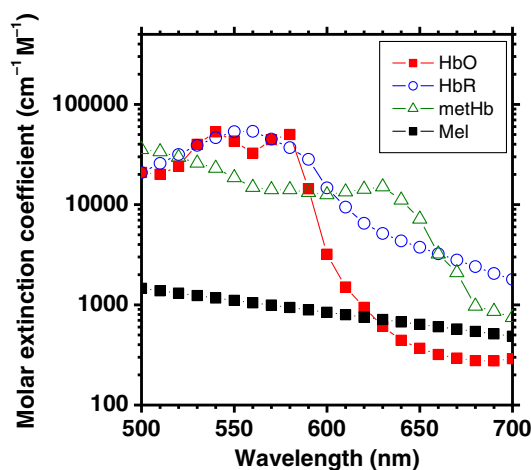

Fig. 1 Extinction coefficient spectra of typical hemoglobin derivatives (oxygenated hemoglobin HbO,[2] deoxygenated hemoglobin HbR,[2] and methemoglobin[3]) and melanin[4] in the visible wavelengths between 500 and 700 nm.

potentially serious methemoglobin levels induced by topical anesthesia with lidocaine and benzocaine.[15,16] As with other potentially life-threatening sicknesses, early assessment of methemoglobinemia is essential for effective monitoring and treatment.

The conventional methods for evaluating methemoglobin in hypoxemic patients are arterial blood gas analysis, pulse oximetry, and CO-oximetry. Arterial blood gas analysis results could show a normal oxygen partial pressure (pO_2) even when there is a high concentration of methemoglobin in the blood. This is because arterial blood gas analysis calculates only the dissolved oxygen and not the actual amount of oxygen molecules bound to hemoglobin in blood.[15] Pulse oximetry measures tissue oxygen saturation at two wavelengths (typically 660 and 940 nm), and reliable results are obtained only in the presence of oxyhemoglobin and deoxyhemoglobin. Methemoglobin absorbs light equally at both wavelengths, resulting in an absorbance ratio of one, which corresponds to an oxygen saturation of ~85%.[19] However, when the level of methemoglobin is high, the result is unreliable, because the pulse oximeter readings remain stable. [19–22] CO-oximetry is a bench-top analysis method for the evaluation of methemoglobin, and it has been used as the traditional detection tool for methemoglobinemia. Although CO-oximetry can be used to monitor the response to treatment for methemoglobinemia, it is costly and requires an invasive procedure for collecting blood samples from patients. Moreover, the testing of arterial blood gas samples by CO-oximetry requires an order from the physician. Thus the use of CO-oximetry for the measurement of methemoglobin concentrations is limited by the frequency of orders from physicians for a sequential blood gas analysis. A more rapid, simple, and cost-effective noninvasive monitoring method may allow clinicians to perform accurate diagnostic tests for methemoglobinemia.[23] A pulse CO-oximeter[24] with a contact probe can measure the percentage of methemoglobin continuously and non-invasively, as well as the percutaneous oxygen saturation. The Masimo Pulse CO-Oximeter (Radical-7, Masimo Corp., Irvine, CA) and The Masimo Pulse oximeter (Radical-5, Masimo Corp., Irvine, CA) have been widely used to measure the percentage of methemoglobin and the percutaneous arterial oxygen saturation (SpO_2), respectively. It has been reported that the Radical-7 had a sensitivity of 97.1% and a specificity of 92.4% for detecting the percentage of methemoglobin $\geq 10\%$ when the arterial oxygen saturation (SaO_2) is >95%,[25] whereas the SpO^2 reading by the Radical-5 showed a sensitivity of 100% and a specificity of 93%.[26] In terms of the prevention of infectious diseases, it is desirable to monitor methemoglobin and oxygen saturation levels in a non-contact manner. The chemical reactions in the heme group can result in remarkable variations in the hemoglobin absorption spectrum in the visible region. Following the oxidative reaction of hemoglobin, a significant increase in absorption occurs in the red zone of the visible spectrum, and methemoglobin has a characteristic absorption peak at 630 nm.[3] Changes in the absorption spectrum due to methemoglobin formation are useful for diagnosis of methemoglobinemia and burn wound staging. Some researchers have demonstrated that optical methods have great potential for the non-invasive *in vivo* monitoring of methemoglobin absorption properties; these methods include broadband diffuse optical spectroscopy[27–30] and photoacoustic imaging.[31,32] Since diffuse reflectance spectroscopy (DRS) can be achieved using simple optical components and apparatuses, it is promising as a non-invasive clinical diagnostic technique. DRS can accurately and simultaneously quantify the *in vivo* concentrations of melanin, oxygenated hemoglobin, and deoxygenated hemoglobin.[33–35] Multispectral and hyperspectral imaging techniques can be used to collect spectral information from each pixel in images, which enables the identification of various physiological conditions in living tissues.[36–38]

In the existing literature, a method has been proposed for the measurements of melanin, oxygenated hemoglobin, and deoxygenated hemoglobin in skin tissues,[35] and it has been applied to multispectral imaging for visualizing spatiotemporal changes in peripheral hemodynamics and pigmentations in response to physiological stimuli.[39] In this approach, multiple regression analysis is performed using the absorbance spectrum of human skin between 500 and 600 nm a s a response variable and the known extinction coefficient spectra of melanin, oxygenated hemoglobin, and deoxygenated hemoglobin as predictor variables to provide multiple regression coefficients. The concentrations of melanin and hemoglobin are then determined from the regression coefficients using empirical formulas that are deduced numerically in advance. A Monte Carlo simulation (MCS) of light transport in a human skin model is carried out to numerically establish the empirical formulas. We leveraged this approach in our study and extended it to

the simultaneous quantification of methemoglobin, oxygenated hemoglobin, and deoxygenated hemoglobin. The purpose of our work was to demonstrate the feasibility of visible spectral diffuse reflectance measurement for *in vivo* monitoring of hemoglobin derivatives and evaluating methemoglobin production and reduction as well as hypoxemia during methemoglobinemia in rats. To confirm the feasibility of the method for quantifying the volume concentrations of methemoglobin, oxygenated hemoglobin, and deoxygenated hemoglobin during methemoglobinemia, we performed *in vivo* animal experiments with rats exposed to sodium nitrite ($NaNO_2$) at different doses.

2 Materials and Methods

2.1 *Animal Preparation*

Male Wister rats ($n = 13$) weighing 300 to 630 g were used for the animal experiments. All experimental procedures were conducted according to the protocols approved by the Animal Care Committee of Tokyo University of Agriculture and Technology (Approval No. 31-75). Anesthesia of rats was performed with isoflurane and maintained at a depth such that the rat had no response to toe pinching. After the induction of anesthesia, the dorsal region was shaved, and a depilatory agent containing thioglycolic acid was applied to the rat dorsal skin. Thirteen rats were administered a rapid single dose of $NaNO_2$ intraperitoneally at the different dose conditions of 25, 37.5, 50, and 75 mg/kg body weight (2-ml dosing volume). Twelve out of thirteen rats were divided into four different dose groups consisting of three rats, respectively, and used only for spectral diffuse reflectance imaging. One out of thirteen rats was used for simultaneous measurements of pulse oximeter signals and spectral diffuse reflectance images.

2.2 *Experimental Apparatus*

Figure 2 shows a schematic illustration of the hyperspectral imaging system used in this study. A halogen lamp light source (LA-150SAE, Hayashi Watch Works Co., Ltd., Tokyo, Japan) was used to illuminate the sample surface via a light guide with a ring-shaped illuminator. Diffusely reflected light was received by a hyperspectral camera (NH-NSD, EBA JAPAN, Tokyo, Japan) with a camera lens to acquire a hyperspectral cube. The hyperspectral camera has an internal optical stage-scanning system consisted of a slit, a collimating lens, a transmission diffraction grating, a relay lens, and a two-dimensional charge-coupled device detector sensor. A line in the scene is imaged onto the slit entrance. After collimation, the transmission diffraction grating splits the light into a series of spectral bands that are then focused onto the detector sensor via the relay lens, where one axis (x axis) records the spatial information (along the slit) and the other axis (z axis) records the spectral information. By scanning the internal optical stage along the direction perpendicular to the slit line, the camera collects two-dimensional images for adjacent lines, creating a hyperspectral cube with two spatial dimensions and one spectral dimension; the first two dimensions were spatial (x and y axes) with 640×480 pixels, whereas the third dimension (z axis) was the wavelength, ranging from 400 to 1000 nm at 10-nm intervals. The total acquisition time for one hyperspectral cube was 13 s. The spectral resolution of the camera is 10 nm. A standard white diffuser with 99% reflectance (SRS-99-020, Labsphere Incorporated, North Sutton, NH, USA) was used to correct for the interinstrument differences in the output of the camera and the spatial non-uniformity of the illumination. A ring-shaped polarizer and an analyzer were set in a crossed Nicols alignment to reduce specular reflection from the skin surface. The hyperspectral image data were then stored on a personal computer and analyzed according to the visualizing process described above. The experiments were performed in the darkroom to prevent the effect of ambient light on the spectral imaging. Therefore, ambient light had no significant effect on the imaging. Simultaneously with the optical imaging of skin tissue, the percutaneous arterial oxygen saturation [SpO_2 (%)], heart rate [HR (bpm)], and pulse distention (PD [(μm)]) were measured for one rat by a pulse oximeter with a foot sensor (MOUSEOX Pulse Oximeter; Star Life Science, Oakmont, PA, USA). The amplitude of the light absorption signal due to the cardiac pulse, which corresponded to the change in distention
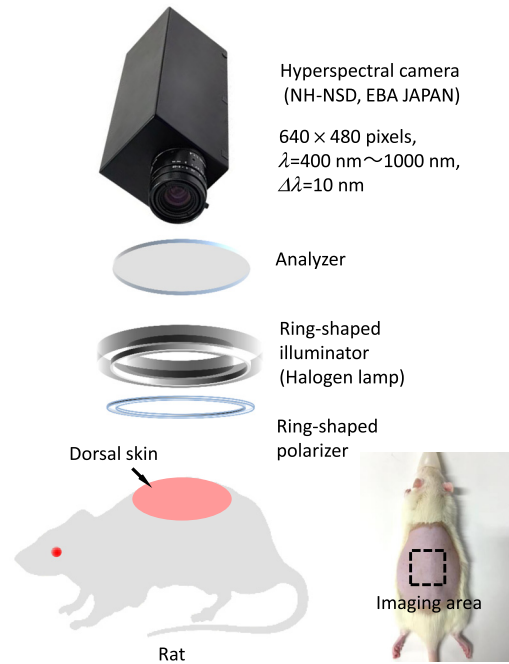
Fig. 2 Flow diagram of the process for estimating the concentration of methemoglobin C_{metHb}, oxygenated hemoglobin C_{HbO}, deoxygenated hemoglobin C_{HbR}, and melanin C_m. (a) Preparation step for establishing the empirical formulas and (b) main process for estimating C_{metHb}, C_{HbO}, C_{HbR}, and C_m from the measured diffuse reflectance spectrum.

of the arterial blood vessels at the sensor location, was taken to be the PD. It can be used as an indicator of local blood flow or peripheral blood volume. After a rest of 5 min, acquisitions of hyperspectral image data were made immediately before the administration of $NaNO_2$ (0 min) and at 5, 10, 20, 30, 60, 120, 40, 300, and 360 min after the administration of $NaNO_2$, whereas recordings of pulse oximeter signals were made for a total of 360 min at 5-s intervals.

2.3 Principle for Quantifying Chromophore Concentrations

2.3.1 Making empirical formulas for quantifying chromophore concentrations

We modified the approach proposed by Nishidate et al.,[35] which was designed to quantify the three major chromophores of oxygenated hemoglobin, deoxygenated hemoglobin, and melanin. We take methemogobin into account in the skin tissue model in addition to oxygenated hemoglobin, deoxygenated hemoglobin, and melanin. Figure 3(a) shows a flow diagram of establishing the empirical formulas for quantifying concentrations of methemoglobin, oxygenated hemoglobin, deoxygenated hemoglobin, and melanin. The attenuation spectrum $A(\lambda)$ was defined as

$$A(\lambda) = \log_{10}\frac{1}{R(\lambda)}, \tag{1}$$

where $R(\lambda)$ is the diffuse reflectance spectrum normalized by the incident light spectrum. Because attenuation due to light scattering can be treated as pseudochromophore,[40,41] the attenuation spectrum $A(\lambda)$ can be approximated as the sum of attenuations due to absorption and scattering in the skin tissue as follows:

$$A(\lambda) = C_{\mathrm{metHb}}l_d(\lambda, C_{\mathrm{metHb}}, C_{\mathrm{HbO}}, C_{\mathrm{HbR}}, \mu_s')\varepsilon_{\mathrm{metHb}}(\lambda) + C_{\mathrm{HbO}}l_d(\lambda, C_{\mathrm{metHb}}, C_{\mathrm{HbO}}, C_{\mathrm{HbR}}, \mu_s')\varepsilon_{\mathrm{HbO}}(\lambda)$$
$$+ C_{\mathrm{HbR}}l_d(\lambda, C_{\mathrm{metHb}}, C_{\mathrm{HbO}}, C_{\mathrm{HbR}}, \mu_s')\varepsilon_{\mathrm{HbR}}(\lambda) + C_{\mathrm{m}}l_e(\lambda, C_{\mathrm{m}}, \mu_s')\varepsilon_{\mathrm{m}}(\lambda) + S(\lambda, \mu_s'), \tag{2}$$
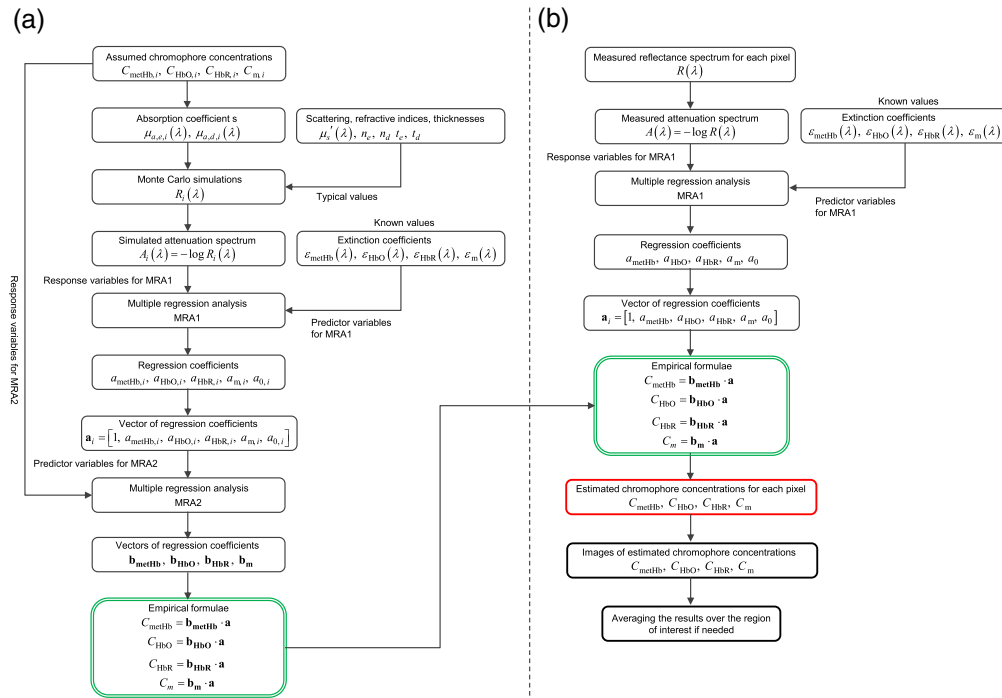
Fig. 3 Schematic illustration of the hyperspectral imaging system.

where C (M) is the molar concentration, l (cm) is the mean path length, $\varepsilon(\lambda)$ $(\text{cm}^{-1}\,\text{M}^{-1})$ is the molar extinction coefficient, and $S(\lambda, \mu_s')$ indicates attenuation due to light scattering in the tissue. The subscripts metHb, HbO, HbR, m, d, and e indicate methemoglobin, oxygenated hemoglobin, deoxygenated hemoglobin, melanin, dermis, and epidermis, respectively. Using $A(\lambda)$ at $\lambda = 550$ to 680 nm at 10-nm intervals as the response variable and $\varepsilon(\lambda)$ at the same wavelength range as the predictor variables, the multiple regression analysis can be performed as

$$A(\lambda) = a_{\text{metHb}}\varepsilon_{\text{metHb}}(\lambda) + a_{\text{HbO}}\varepsilon_{\text{HbO}}(\lambda) + a_{\text{HbR}}\varepsilon_{\text{HbR}}(\lambda) + a_m\varepsilon_m(\lambda) + a_0, \qquad (3)$$

where a_{metHb}, a_{HbO}, a_{HbR}, a_m, and a_0 are the regression coefficients. We refer to this multiple regression analysis as MRA1. In the wavelength range 550 to 680 nm, oxygenated hemoglobin and deoxygenated hemoglobin have isosbestic points at 570 and 585 nm. Oxygenated hemoglobin and methemoglobin have an isosbestic point at 590 nm. Deoxygenated hemoglobin and methemoglobin have isosbestic points around 590 and 660 nm. Reflectance at 560 nm is sensitive to the oxygen state of hemoglobin. Therefore, we chose the wavelength range 550 to 680 nm to use for the multiple regression analysis. As described in Sec. 2.4, we used a hyperspectral camera with a 10-nm spectral resolution in this study. Therefore, we used a spectrum with 10-nm-intervals for this multiple regression analysis. The multiple regression coefficients a_{metHb}, a_{HbO}, a_{HbR}, and a_m describe the degree of contribution of $\varepsilon_{\text{metHb}}(\lambda)$, $\varepsilon_{\text{HbO}}(\lambda)$, $\varepsilon_{\text{HbR}}(\lambda)$, and $\varepsilon_m(\lambda)$, respectively, to $A(\lambda)$. Therefore, the values of a_{metHb}, a_{HbO}, a_{HbR}, and a_m are related to the products of chromophore concentrations and mean optical path lengths. We used the multiple regression coefficients a_{metHb}, a_{HbO}, a_{HbR}, a_m, and a_0 to estimate the concentrations of C_{metHb}, C_{HbO}, C_{HbR}, and C_m. For this purpose, we assumed the empirical formulas for C_{metHb}, C_{HbO}, C_{HbR}, and C_m as

$$C_{\text{metHb}} = \mathbf{b}_{\text{metHb}} \cdot \mathbf{a}, \qquad (4)$$

$$C_{\text{HbO}} = \mathbf{b}_{\text{HbO}} \cdot \mathbf{a}, \qquad (5)$$

$$C_{\text{HbR}} = \mathbf{b}_{\text{HbR}} \cdot \mathbf{a}, \qquad (6)$$

$$C_{\text{m}} = \mathbf{b}_{\text{m}} \cdot \mathbf{a}, \qquad (7)$$

where

$$\mathbf{a} = [1, a_{\text{metHb}}, a_{\text{HbO}}, a_{\text{HbR}}, a_m, a_0]^{\text{T}}, \tag{8}$$

$$\mathbf{b}_{\text{metHb}} = [b_{\text{metHb},0}, b_{\text{metHb},1}, b_{\text{metHb},2}, b_{\text{metHb},3}, b_{\text{metHb},4}, b_{\text{metHb},5}], \tag{9}$$

$$\mathbf{b}_{\text{HbO}} = [b_{\text{HbO},0}, b_{\text{HbO},1}, b_{\text{HbO},2}, b_{\text{HbO},3}, b_{\text{HbO},4}, b_{\text{HbO},5}], \tag{10}$$

$$\mathbf{b}_{\text{HbR}} = [b_{\text{HbR},0}, b_{\text{HbR},1}, b_{\text{HbR},2}, b_{\text{HbR},3}, b_{\text{HbR},4}, b_{\text{HbR},5}], \tag{11}$$

$$\mathbf{b}_{\text{m}} = [b_{\text{m},0}, b_{\text{m},1}, b_{\text{m},2}, b_{\text{m},3}, b_{\text{m},4}, b_{\text{m},5}]. \tag{12}$$

The symbol $[]^{\text{T}}$ represents the transposition of a vector. The coefficient vectors $\mathbf{b}_{\text{metHb}}$, $\mathbf{b}_{\text{HbO}}$, $\mathbf{b}_{\text{HbR}}$, and $\mathbf{b}_m$ are unknown and must be determined before estimating C_{metHb}, C_{HbO}, C_{HbR}, and C_m. We conducted further multiple regression analyses to establish the vectors $\mathbf{b}_{\text{metHb}}$, $\mathbf{b}_{\text{HbO}}$, $\mathbf{b}_{\text{HbR}}$, and $\mathbf{b}_m$. In this second multiple regression analysis, C_{metHb}, C_{HbO}, C_{HbR}, and C_m were regarded as response variables, and the five regression coefficients (a_{metHb}, a_{HbO}, a_{HbR}, a_m, and a_0) that were obtained from MRA1 were regarded as predictor variables to determine the empirical formulas for C_{metHb}, C_{HbO}, C_{HbR}, and C_m. We refer to this analysis as MRA2.

We used the MCML software developed by Wang et al.[42] for the MCS to simulate the diffuse reflectance spectra of skin tissues. The simulated spectra were used to derive the datasets of chromophore concentrations and the multiple regression coefficients of a_{metHb}, a_{HbO}, a_{HbR}, a_m, and a_0. The simulation model consisted of two layers representing the epidermis and dermis. 5,000,000 photon packets were launched in a single simulation of diffuse reflectance at each wavelength. The absorption coefficients of oxygenated hemoglobin $\mu_{a,\text{HbO}}(\lambda)$ (cm^{-1}), deoxygenated hemoglobin $\mu_{a,\text{HbR}}(\lambda)$ (cm^{-1}), methemoglobin $\mu_{a,\text{metHb}}(\lambda)$ (cm^{-1}), and melanin $\mu_{a,m}(\lambda)$ (cm^{-1}) were obtained from the values of $\varepsilon_{\text{HbO}}(\lambda)$ (cm^{-1} M^{-1}), $\varepsilon_{\text{HbR}}(\lambda)$ (cm^{-1} M^{-1}), $\varepsilon_{\text{metHb}}(\lambda)$ (cm^{-1} M^{-1}), and $\varepsilon_{\text{mel}}(\lambda)$ (cm^{-1} M^{-1}) as shown in Fig. 1. The value of $\mu_a(\lambda)$ (cm^{-1}) was derived from the product of the molar concentration C (M) and the molar extinction coefficient $\varepsilon(\lambda)$ (cm^{-1} M^{-1}) as, $\mu_a(\lambda) = 2.303 C \varepsilon(\lambda)$. The absorption coefficients $\mu_{a,m}(\lambda)$ for 10 different melanin concentrations were input for the epidermis layer in the MCS as $C_m = 1$ to 10 vol. % at 1-vol. % intervals. We assumed that the whole blood with 2.32 mM of hemoglobin is 100% volume concentration of total hemoglobin ($C_{\text{HbT}} = 100$ vol. %). The sum of the absorption coefficients of oxygenated hemoglobin $\mu_{a,\text{HbO}}(\lambda)$, deoxygenated hemoglobin $\mu_{a,\text{HbR}}(\lambda)$, and methemoglobin $\mu_{a,\text{metHb}}(\lambda)$ represents the absorption coefficients of total hemoglobin $\mu_{a,\text{HbT}}(\lambda)$ (cm^{-1}). The absorption coefficients for total hemoglobin $\mu_{a,\text{HbT}}(\lambda)$ for the values of $C_{\text{HbT}} = 0.2$ to 1.0 vol. % at 0.2-vol. % intervals were input for the dermis layer in the MCS. Tissue oxygen saturation (StO$_2$) and methemoglobin saturation (StMet) were determined by $\mu_{a,\text{HbO}}(\lambda)/\mu_{a,\text{HbT}}(\lambda)$ and $\mu_{a,\text{metHb}}(\lambda)/\mu_{a,\text{HbT}}(\lambda)$, respectively, and values ranged from 0% to 100% were used for the simulation. The refractive index of the epidermis and dermis layers was assumed to be same and fixed at 1.4. The thicknesses of epidermis and dermis layers were set to 0.06 and 4.94 mm, respectively. The reduced scattering coefficient $\mu_s'(\lambda)$(cm^{-1}) calculated from the typical values for the scattering coefficient[35] $\mu_s(\lambda)$ (cm^{-1}) and anisotropy factor[35] $g(\lambda)$ were used for both epidermis and dermis layers. The value of μ_s' at 550 nm was 31.62 cm^{-1}. In total, 1550 diffuse reflectance spectra at $\lambda = 550$ to 680 nm at 10-nm intervals were simulated under the various combinations of C_{metHb} vol. %, C_{HbO} vol. %, C_{HbR} vol. %, and C_m vol. %. The MRA1 analysis for each simulated spectrum generated 1550 sets of vector $\mathbf{a}$ and concentrations of C_{metHb} vol. %, C_{HbO} vol. %, C_{HbR} vol. %, and C_m vol. %. The coefficient vectors $\mathbf{b}_{\text{metHb}}$, $\mathbf{b}_{\text{HbO}}$, $\mathbf{b}_{\text{HbR}}$, and $\mathbf{b}_m$ were determined statistically by performing MRA2. In this way, we used both multiple regression analysis and the MCS together to establish the empirical model.

2.3.2 Estimating chromophore concentrations using the established empirical formulas

Figure 3(b) shows the main process for estimating concentrations of methemoglobin, oxygenated hemoglobin, deoxygenated hemoglobin, and melanin from the measured diffuse reflectance

spectrum using the established empirical formulas. The measured diffuse reflectance spectrum $R(\lambda)$ is converted into the attenuation spectrum $A(\lambda)$. MRA1 is then performed using the measured $A(\lambda)$ at $\lambda = 550$ to 680 nm at 10-nm intervals as the response variable and $\varepsilon(\lambda)$ at the same wavelength range as the predictor variables. The resultant multiple regression coefficients a_{metHb}, a_{HbO}, a_{HbR}, a_m, and a_0 are substituted into the empirical formulas established in the preparation step described in Sec 2.3.1 and finally the estimated concentrations of methemoglobin C_{metHb} vol. %, oxygenated hemoglobin C_{HbO} vol. %, deoxygenated hemoglobin C_{HbR} vol. %, and melanin C_m vol. % are obtained. The above procedure was done for each pixel.

2.4 *In Silico Experiments*

We performed *in silico* experiments with diffuse reflectance samples generated by the MCS to validate the accuracy of the proposed method. For test samples, the values of C_{HbT} were set to 0.3, 0.5, and 0.7 vol. %, whereas those of C_m were set to 1.5, 3.5, and 5.5 vol. % The values of StO_2 were ranged from 2% to 72%, whereas those of StMet were set to 20%, 50%, and 80%. Other conditions for the MCS were fixed to be the same as those in Sec. 2.3.1. In total, 81 diffuse reflectance spectra at $\lambda = 550$ to 680 nm at 10-nm intervals were generated under the combinations of C_{HbT}, C_m, StO_2, and StMet.

2.5 *Statistical Analysis*

To assess the results from *in silico* experiments, Pearson's correlation coefficient and root-mean-square error (RMSE) were calculated using the ground truth values and estimated values by the proposed method. A probability value of $p < 0.05$ indicates statistical significance. We used only one area of each rat for data analysis of hyperspectral images. Region of interest (ROI) of 300×300 pixels was set in each image and the mean and the standard deviation (SD) over the ROI were calculated for the analysis of time courses in C_{metHb} C_{HbO}, C_{HbR}, C_{HbT} C_m, StO_2, and StMet. Therefore, data are expressed as mean $\pm$ SD. In order to compare the difference in each parameter across the dose conditions, the mean over the three rats in each group was also calculated.

3 Results and Discussion

We first validated the accuracy of the proposed method by *in silico* experiments with diffuse reflectance samples generated by the MCS (Fig. 4). The estimated and ground truth values for
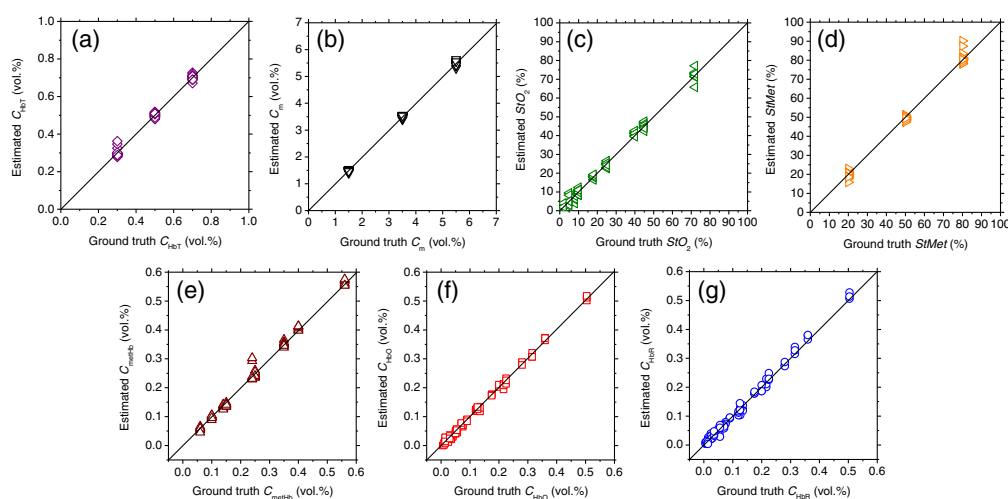

Fig. 4 Comparisons between the estimated and ground truth values for (a) total hemoglobin concentration C_{HbT}; (b) melanin concentration C_m; (c) tissue oxygen saturation StO_2; (d) methemoglobin saturation StMet; (e) methemoglobin concentration C_{metHb}; (f) oxygenated hemoglobin concentration C_{HbO}; and (g) deoxygenated hemoglobin concentration C_{HbR}, obtained from the *in silico* experiments.
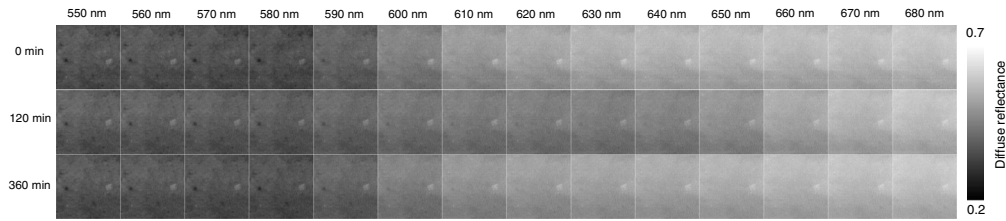
Fig. 5 Typical spectral diffuse reflectance images of rat dorsal skin measured by the hyperspectral camera at 0, 120, and 360 min after the administration of $NaNO_2$. Three representative time points are illustrated to show the largest differences, i.e., at 120 min the diffuse reflectance at 610 to 650 nm was the lowest.

total hemoglobin concentration C_{HbT}, melanin concentration C_m, tissue oxygen saturation StO_2, methemoglobin saturation StMet, methemoglobin concentration C_{metHb}, oxygenated hemoglobin concentration C_{HbO}, and deoxygenated hemoglobin concentration C_{HbR} are shown in Figs. 4(a)–(g), respectively. The estimated values are well correlated with the ground truth values for given ranges of each parameter. The value of Pearson's correlation coefficient between the estimated and ground truth values of C_{HbT}, C_m, StO_2, StMet, C_{metHb}, C_{HbO}, and C_{HbR} were calculated to be 0.997 ($p < 0.0001$), 0.999 ($p < 0.0001$), 0.997 ($p < 0.0001$), 0.998 ($p < 0.0001$), 0.996 ($p < 0.0001$), 0.998 ($p < 0.0001$), and 0.997 ($p < 0.0001$), respectively. The RMSEs of C_{HbT}, C_m, StO_2, StMet, C_{metHb}, C_{HbO}, and C_{HbR} were 0.39%, 0.18%, 3.06%, 0.45%, 0.70%, 3.03%, and 2.21%, respectively.

We examined the spectral diffuse reflectance images obtained from rat dorsal skin at 0, 120, and 360 min after the administration of $NaNO_2$ to confirm the impact of light absorption by methemoglobin on the spectrum. As expected from the absorption spectrum of methemoglobin shown in Fig. 1, the diffuse reflectance values in the range from 610 to 650 nm were clearly decreased at 120 min after the administration of $NaNO_2$ (Fig. 5). We found that an increase in metHb caused by $NaNO_2$ administration would lead to a maximum percentage decrease of 17% in diffuse reflectance at 630 nm [Fig. 6 (c)]. The diffuse reflectance at 520 nm showed that there was an initial slight increase of 2% at 5 min, followed by a decrease of 5% with a minimum value at 120 min, then it returned to its normal level at 360 min [Fig. 6 (c)]. A decrease in R_{560}/R_{570}, i.e., the local peak of the diffuse reflectance at 560 nm relative to that at 570 nm at 10 to 60 min after $NaNO_2$ administration reflected the deoxygenation of hemoglobin [Fig. 6 (d)]. Methemoglobin, oxygenated hemoglobin, and deoxygenated hemoglobin have almost the same molar extinction coefficient at 520 nm, as shown in Fig. 1. Therefore, the change in diffuse reflectance at 520 nm implied a temporary increase in the volume concentration of total hemoglobin.

We applied the proposed method to the spectral diffuse reflectance images obtained from rat dorsal skin before and after the administration of $NaNO_2$ at a dose of 50 mg/kg to evaluate quantitatively changes in chromophore concentrations. Figure 7 shows typical sequential images of (a) C_{metHb}, (b) C_{HbO}, (c) C_{HbR}, (d) StMet, (e) StO_2, (f) C_{HbT}, and (g) C_m obtained from rat dorsal skin before and after the administration of $NaNO_2$ at a dose of 50 mg/kg. Figure 8 shows the typical time courses of (a) C_{metHb}, (b) C_{HbO}, (c) C_{HbR}, (d) StMet, (e) StO_2, (f) C_{HbT}, and (g) C_m averaged over the entire region of each corresponding image shown in Fig. 7. Both C_{metHb} and StMet increased after the administration of $NaNO_2$, whereas C_{HbO} and C_{HbR} decreased and increased, respectively, which was indicative of temporary methemoglobinemia. At 360 min after the administration of $NaNO_2$, both C_{metHb} and StMet returned to their normal levels due to the self-reductive systems of the rat. The value of StO_2 decreased after the administration of $NaNO_2$, indicating temporary hypoxemia caused by methemoglobinemia as expected (Figs. 7 and 8). The value of C_{HbT} showed an initial decrease of 0.03 vol. %, followed by a profound increase of 0.16 vol. % after the administration of $NaNO_2$. The first phase of total hemoglobin change coincided with the decrease in both C_{HbO} and C_{HbR} (Fig. 8).

To confirm the applicability of the method to imaging applications in monitoring of hemoglobin derivatives, we investigated variations in spatial distributions of C_{metHb}, C_{HbO}, C_{HbR}, StMet, StO_2, and C_{HbT}. Figure 9 shows segmentation results for sequential images shown in
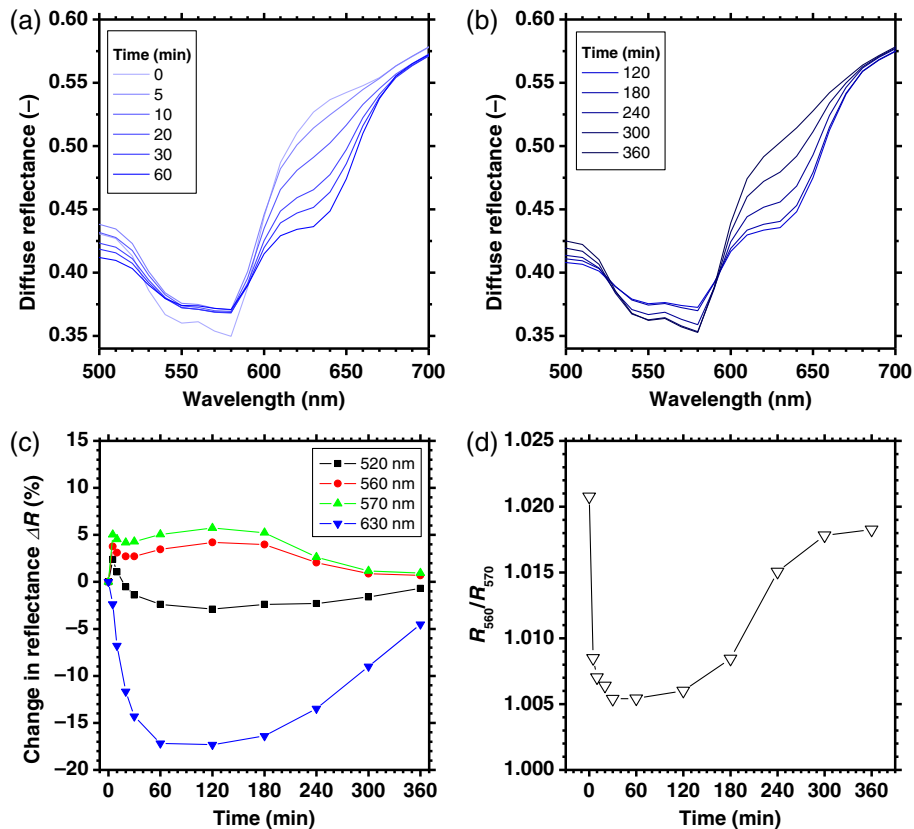
Fig. 6 Typical time course of diffuse reflectance spectra obtained from rat dorsal skin before and after the administration of $NaNO_2$ for (a) 0 to 60 min and (b) 120 to 360 min. Each spectrum is the average value over the ROI in the spectral diffuse reflectance image measured by the hyper spectral camera. (c) The percent change in diffuse reflectance relative to the value at 0 min for 520, 560, 570, and 630 nm. (d) Time course of the ratio of diffuse reflectance at 560 nm and that at 570 nm.

Fig. 7. We selected a threshold pixel value for each chromophore image, and segmented all pixels above the threshold value, and looked at how the segmented regions change over time. The average values overall pixels of images at 0 min after the administration of $NaNO_2$ were selected as the threshold pixel values for C_{HbO}, C_{HbR}, and StO_2, whereas those at 120 min after the administration of $NaNO_2$ were selected as the threshold pixel values for C_{metHb}, C_{HbT}, and StMet. The threshold pixel values for C_{metHb}, C_{HbO}, C_{HbR}, StMet, StO_2, and C_{HbT} were 0.24 vol. %, 0.085 vol. %, 0.05 vol. %, 82%, 65%, and 0.3 vol. %, respectively. The region of segmented pixels for C_{HbT} began to increase in the upper half of the image at 30 min after the administration of $NaNO_2$ and spreads to the lower half of the image until 120 min after the administration of $NaNO_2$ [Fig. 9(f)]. The same tendency can be observed in the segmented image of C_{metHb} [Fig. 9(a)]. On the other hand, the decreases in the regions of segmented pixels for both C_{HbO} and C_{HbR} spread from the upper side to the lower side of the image until 120 min after the administration of $NaNO_2$ [Figs. 9(b) and 9(c)]. The cause of the variations in spatial distribution of C_{metHb}, C_{HbO}, C_{HbR}, and C_{HbT} is unclear. One possible explanation for those variations is heterogeneous microvascular perfusion distribution. Changes in the regions of segmented pixels for StMet are spatially uniform, which is probably due to that StMet is calculated as the ratio of methemoglobin to total hemoglobin [Fig. 9(d)]. The same applies to the segmentation image of StO_2 that is the ratio of oxygenated hemoglobin to total hemoglobin [Fig. 9(e)].

We compared the time courses of (a) C_{metHb}, (b) C_{HbT}, (c) StMet, and (d) StO_2 for $NaNO_2$ doses of 25, 37.5, 50, and 75 mg/kg to investigate the dose-dependent effects of $NaNO_2$ (Fig. 10). The values of C_{metHb} and StMet rapidly increased with a half-maximum time of <20 min, and the time required to return to the normal levels increased proportionally with the dose [Figs. 10(a) and 10(c)]. On the other hand, at each dose condition, the time course of StO_2
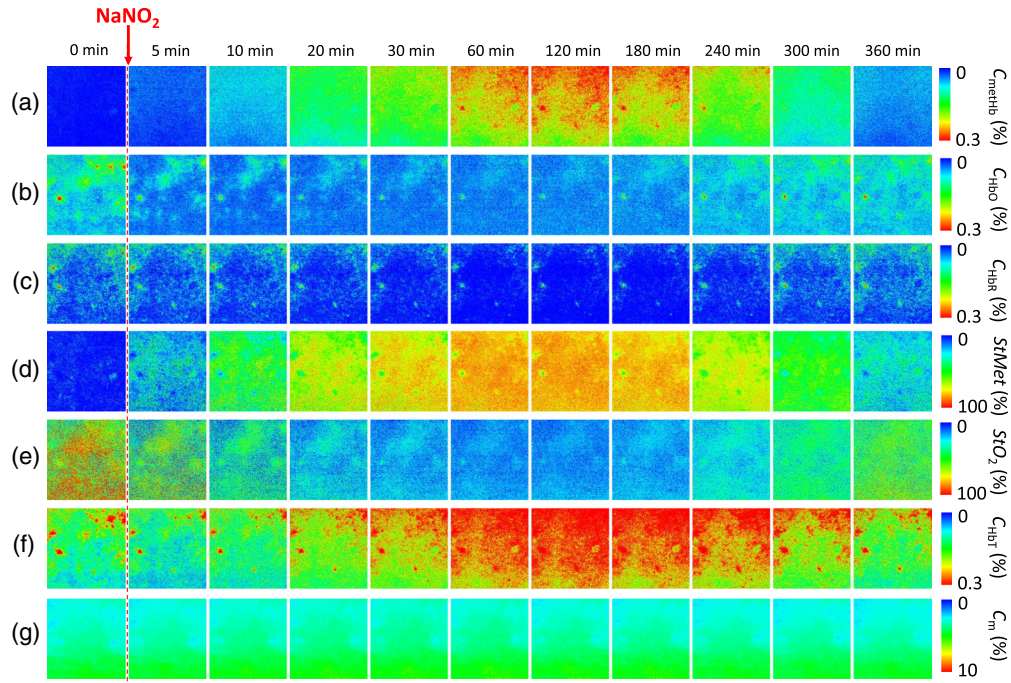
Fig. 7 Typical sequential images of (a) methemoglobin concentration C_{metHb}; (b) oxygenated hemoglobin concentration C_{HbO}; (c) deoxygenated hemoglobin concentration C_{HbR}; (d) methemoglobin saturation StMet; (e) tissue oxygen saturation StO_2; (f) total hemoglobin concentration C_{HbT}; and (g) melanin concentration C_m obtained from rat dorsal skin before and after the administration of $NaNO_2$ at a dose of 50 mg/kg. Data were measured by the proposed method.
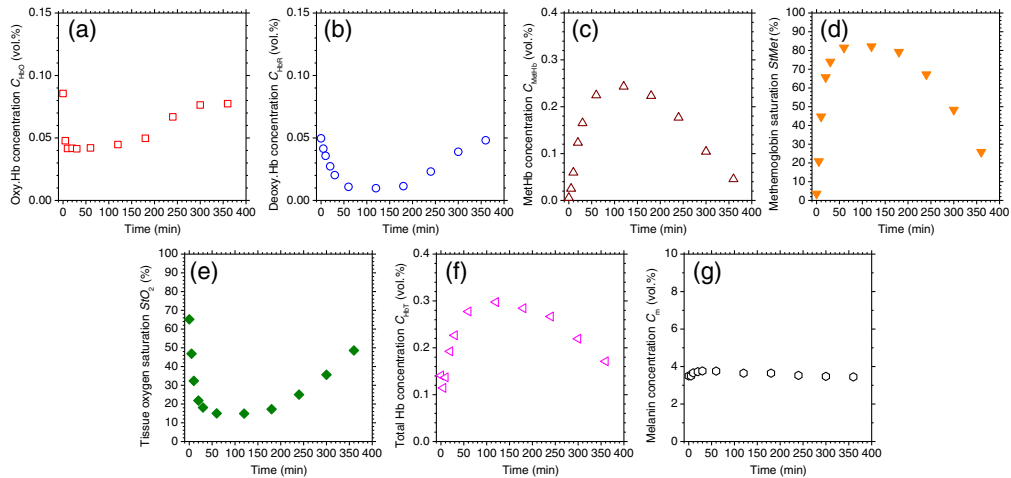

Fig. 8 Typical time courses of (a) methemoglobin concentration C_{metHb}; (b) oxygenated hemoglobin concentration C_{HbO}; (c) deoxygenated hemoglobin concentration C_{HbR}; (d) methemoglobin saturation StMet; (e) tissue oxygen saturation StO_2; (f) total hemoglobin concentration C_{HbT}; and (g) melanin concentration C_m averaged over the entire region of each corresponding image shown in Fig. 7.

dramatically dropped at 60 min after the administration of $NaNO_2$, and then gradually increased again [Fig. 10(d)]. The minimum averaged values of StO_2 during methemoglobinemia were $33.7\% \pm 0.4\%$, $23.1\% \pm 5.6\%$, $8.8\% \pm 1.7\%$, and $9.7\% \pm 5.1\%$ on average for $NaNO_2$ doses of 25, 37.5, 50, and 75 mg/kg, respectively. The values of StO_2 were negatively correlated to those of C_{metHb} and StMet. All three rats with the dose condition of 75 mg/kg body weight died at
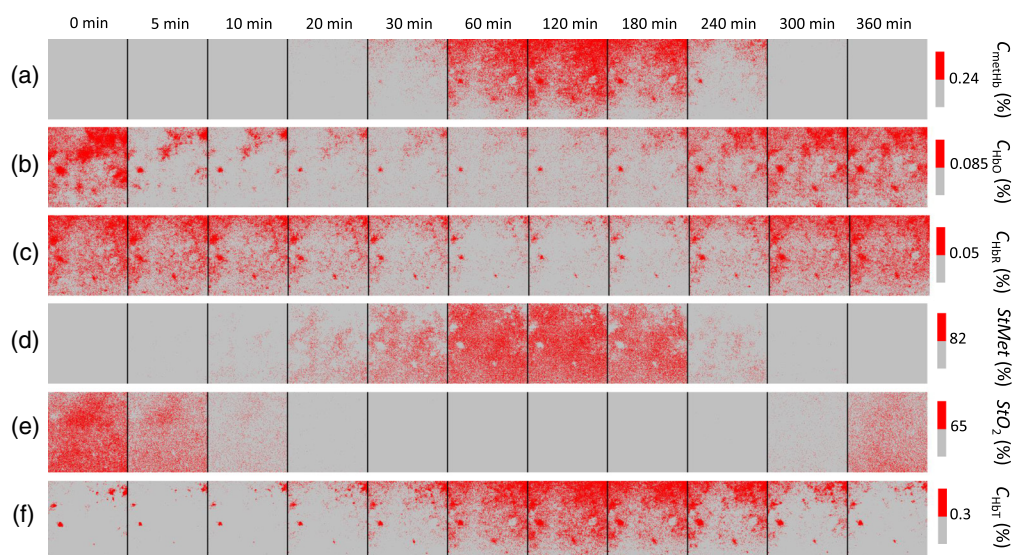
Fig. 9 Segmentation results for sequential images shown in Fig. 7. (a) methemoglobin concentration C_{metHb}; (b) oxygenated hemoglobin concentration C_{HbO}; (c) deoxygenated hemoglobin concentration C_{HbR}; (d) methemoglobin saturation StMet; (e) tissue oxygen saturation StO_2; and (f) total hemoglobin concentration C_{HbT}. Red color and gray color show a pixel above and below a threshold, respectively. The average values overall pixels of images at 0 min were selected as the threshold pixel values for C_{HbO}, C_{HbR}, and StO_2, whereas those at 120 min were selected as the threshold pixel values for C_{metHb}, C_{HbT}, and StMet. The threshold pixel values for C_{metHb}, C_{HbO}, C_{HbR}, StMet, StO_2, and C_{HbT} were 0.24 vol. %, 0.085 vol. %, 0.05 vol. %, 82%, 65%, and 0.3 vol. %, respectively.

60 to 69 min after the administration of $NaNO_2$, whereas those with the other dose conditions survived. Therefore, the median lethal dose was speculated to be within the dose of 50 to 75 mg/kg. We found that the maximum value of StMet increased with increasing dose up to 50 mg/kg, in which it reached a plateau [Fig. 10 (e)].

In order to discuss the results of total hemoglobin concentration C_{HbT} after the administration of $NaNO_2$, we compared the time course of C_{HbT} obtained by the proposed method with HR and pulse distension (PD) measured by the commercial existing pulse oximeter [Figs. 11(a) and 11(b)]. We found that the HR significantly increased to a maximum of 323 bpm at 135 min after the administration of $NaNO_2$, then it gradually decreased for 210 min [Fig. 11(a)]. This increase in HR corresponded to tachycardia, which is a symptom of methemoglobinemia.[43] The PD after the administration of $NaNO_2$ initially decreased to 9.3 μm, but then it significantly increased to a maximum of 76.2 μm at 63 min, then subsequently returned to normal levels [Fig. 11(b)]. The profound increase in PD indicated an elevated cardiac output caused by tachycardia and the resultant increase in peripheral blood volume to compensate for the hypoxia and hypoxemia during methemoglobinemia; this was in agreement with the time course of C_{HbT} obtained by the proposed method.

We also compared the time course of StO_2 obtained by the proposed method with percutaneous arterial oxygen saturation SpO_2 measured by the commercial existing pulse oximeter. We found that the SpO_2 significantly dropped after the administration of $NaNO_2$, then remained around 82.5% for 160 min [Fig. 11(c)]. This observation was in agreement with several reports of SpO_2 measured by conventional pulse oximetry during methemoglobinemia.[19–22] It has been reported that methemoglobinemia can cause a discrepancy between the values of SpO_2 measured by a conventional pulse oximeter and the actual arterial oxygen saturation (SaO_2) calculated by arterial blood gas measurement.[19–22] The values of SpO_2 are not proportional to the actual SaO_2 during methemoglobinemia, since elevated methemoglobin levels (up to 60%) force the SpO_2 value to be around 85%, whereas SaO_2 reaches $\sim$35%.[19] When methemoglobin is elevated, the SpO_2 values measured by conventional pulse oximetry are inaccurate and can falsely diagnose the actual status of patients.
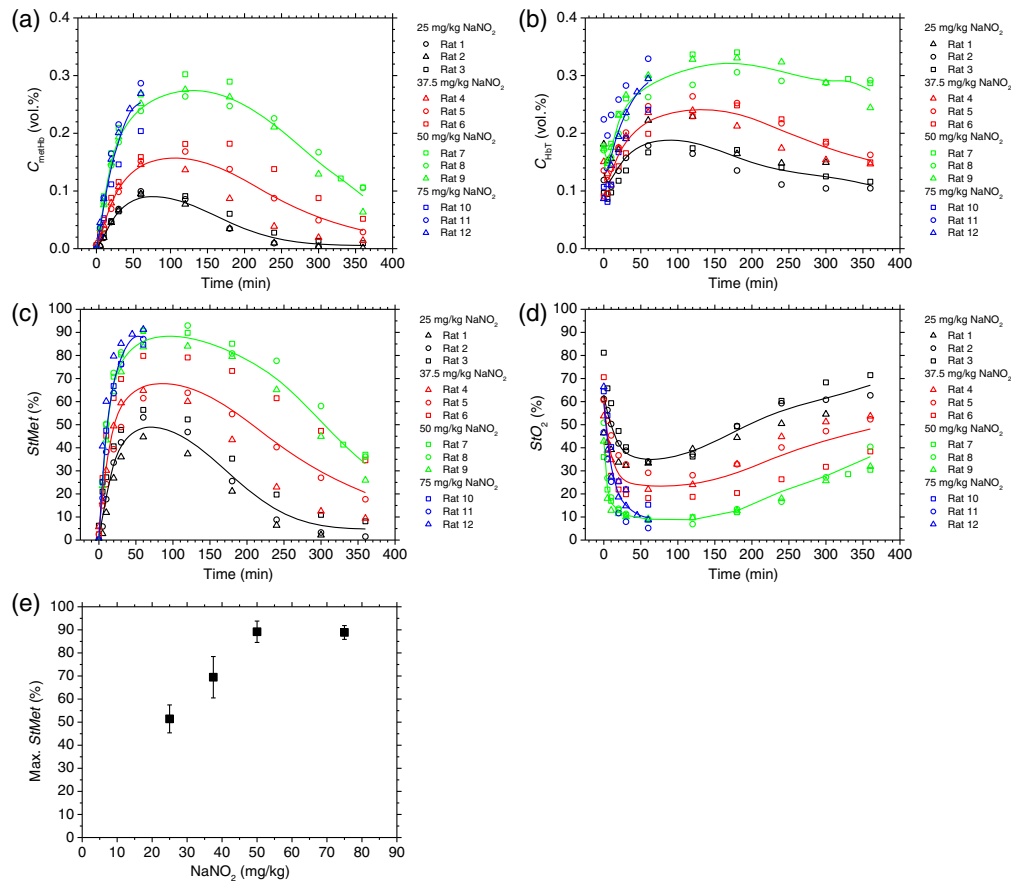
Fig. 10 Time courses of (a) methemoglobin concentration C_{metHb}; (b) total hemoglobin concentration C_{HbT}; (c) methemoglobin saturation StMet; and (d) tissue oxygen saturation StO_2 for various doses of $NaNO_2$. (e) Relationship between the maximum value of StMet and the $NaNO_2$ dose. Data were obtained by the proposed method. Solid lines in (a)–(d) are means of three rats for each dose group. Plots and error bars in (e) show means and SDs of three rats for each dose group.

In contrast, the values of StO_2 obtained by the proposed method were dramatically decreased with a minimum of 19.9% as shown in Fig. 11(c). Since the value of StO_2 estimated by the proposed method represents the oxygen saturation for a mixture of SaO_2 and SvO_2, it should be calculated to be lower than the SaO_2 value. Considering that the SaO_2 value has been reported to be ~35%during methemoglobinemia,[19] it is reasonable that the minimum averaged values of StO_2 during methemoglobinemia showed $33.7\% \pm 0.4\%$, $23.1\% \pm 5.6\%$, $8.8\% \pm 1.7\%$, and $9.7\% \pm 5.1\%$ on average for $NaNO_2$ doses of 25, 37.5, 50, and 75 mg/kg, respectively, as shown in Fig. 10(d). The results for StO_2 indicated that the proposed method can be used to evaluate hypoxemia during methemoglobinemia.

The advantage of the diffuse reflectance imaging over the DRS is the ability to visualize the spatial distribution of chromophores. For example, the spatial distributions of oxygenated hemoglobin concentration, deoxygenated hemoglobin concentration, methemoglobin concentration, and tissue oxygen saturation are important for evaluating the depth of burn injury to classify the severity of burn injury. This issue should be studied further in the future. Near-infrared spectroscopy measurements[29–32] also considered lipids and water as major chromophores in addition to hemoglobin derivatives because lipids and water have distinct absorption peaks in the near-infrared wavelength region. On the other hand, there is no significant absorption by lipids or water in the wavelength range from 550 to 680 nm we used. Therefore, we did not consider lipids and water as major chromophores in this study. The current empirical formulas for chromophores were derived from the MCS with a typical reduced scattering coefficient spectrum.
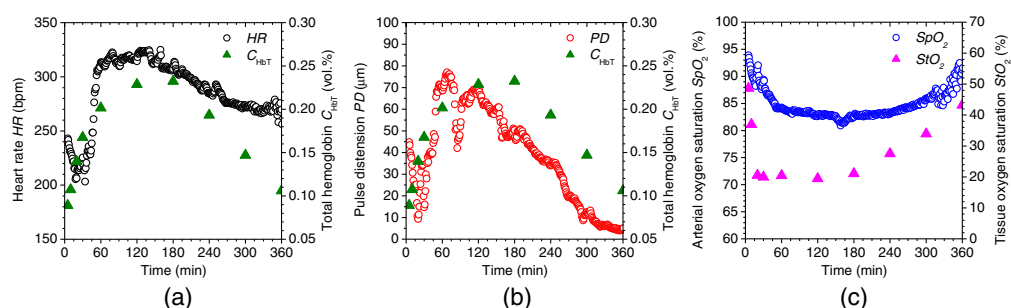
Fig. 11 Time courses of (a) HR and total hemoglobin concentration C_{HbT}; (b) PD and total hemoglobin concentration C_{HbT}; and (c) percutaneous arterial oxygen saturation SpO_2 and tissue oxygen saturation StO_2 for rat after the administration of $NaNO_2$ at a dose of 37.5 mg/kg. HR, PD, and SpO_2 were measured by the commercial existing pulse oximeter, whereas C_{HbT} and StO_2 were obtained by the proposed method.

However, the reduced scattering coefficient spectrum usually differs among body parts and may vary with the age of the subjects. Correct estimation of the scattering properties or consideration of the variations in the reduced scattering coefficient spectrum is essential to precisely estimate the chromophore concentrations. We assumed the typical thicknesses of epidermis and the dermis in the MCS to establish the empirical model. The assumed epidermis and dermis thicknesses could have an impact to the results. The probability that light is absorbed by melanin in the epidermis will be higher than the probability that light is absorbed by hemoglobin in the dermis as epidermis becomes thicker. Therefore, if the thickness of epidermis is larger than the typical value, melanin concentration in epidermis or hemoglobin derivatives concentrations may be under- or overestimated, respectively. The full thickness of the skin tissue model was set to 5 mm in the MCS. The simulated diffuse reflectance could be increased if the total thickness of skin tissue model is larger than 5 mm. Hence, the MCS on a thicker tissue model with a semi-infinite geometry could change the results. However, the possibility of relative measurements of oxygenated hemoglobin, deoxygenated hemoglobin, methemoglobin, and melanin in the skin tissue could still prove valuable. Although we did not consider the polarized photons in the MCS, the diffuse reflectance was calculated separately from the specular reflectance in the simulation and used for in a data set for the empirical model. The quantification accuracy may be improved by taking into account the polarization effects in the MCS. We performed the MCS using the MCML software. The MCML software basically output the physical quantities of photon absorption, fluence, diffuse reflectance, specular reflectance, and total transmittance. It could be possible to estimate the mean path length if we modified the MCML source code. The estimated mean path length should be compared with the values of **a** and **b** in the future. The present method lacks depth resolution, because it relies on the integration of all diffusing reflection information along the depth direction. Moreover, the present method is based on the MCS model, which assumes uniformly distributed scattering and absorption properties. The current algorithm performs the multiple regression analysis using each pixel in the spectral image to calculate the multiple regression coefficients. This process is relatively time-consuming, and the computational load increases when the number of pixels in an image for analysis increases. Therefore, this method may not be suitable for real-time high temporal and spatial resolution imaging of chromophores *in vivo*. Although hyperspectral imaging techniques have been widely used for scientific purposes in the laboratory environment, it is impractical for clinical use due to the large size and high cost of commercial setups. It is advantageous that the proposed algorithm can also be combined with the RGB camera-based spectral image reconstruction technique based on the Wiener estimation method.[44] This is promising for the establishment of a compact and affordable imaging system that can simultaneously evaluate the spatiotemporal distributions of methemoglobin, oxygenated hemoglobin, and deoxygenated hemoglobin in clinical point-of-care testing. Such a device would have an enormous impact on the health of people of all ages worldwide, and this issue should be studied further in the future.

4 Conclusions

In summary, this study demonstrated the usefulness of a new non-contact measuring method based on DRS for the simultaneous evaluations of the precutaneous volume concentrations of methemoglobin, oxygenated hemoglobin, deoxygenated hemoglobin, and melanin as well as tissue oxygen saturation and methemoglobin saturation. *In vivo* experiments with rat dorsal skin before and after the administration of $NaNO_2$ at doses of 25, 37.5, 50, and 75 mg/kg were performed to induce methemoglobinemia. Both the methemoglobin concentration and methemoglobin saturation rapidly increased with a half-maximum time of <20 min. They reached their maximal values nearly 60 min after the administration of $NaNO_2$, and the time required to return to the normal levels increased proportionally with the dose, which implied that the methemoglobinemia was temporary. The values of tissue oxygen saturation dramatically dropped after the administration of $NaNO_2$, and then they gradually increased for each dose condition, indicating temporary hypoxemia caused by methemoglobinemia. The time course of the peripheral volume concentration of total hemoglobin during methemoglobinemia obtained by the proposed method reflects both the HR and PD that are measured by the commercially available pulse oximeter. The results of this study showed that the proposed method has potential for the simultaneous evaluations of the methemoglobin level, regional peripheral blood volume, and hypoxemia during methemoglobinemia.

Disclosures

The authors declare no conflicts of interest.

Acknowledgments

References

1. A. N. Yaroslavsky et al., "Optics of Blood," in *Handbook of Optical Biomedical Diagnostics*, V. V. Tuchin, Ed., SPIE Press, Bellingham, Washington (2002).
2. S. A. Prahl, "Tabulated molar extinction coefficient for hemoglobin in water," 1999, http://omlc.ogi.edu/spectra/hemoglobin/summary.html
3. W. G. Zijlstra and A. Buursma, "Spectrophotometry of hemoglobin: absorption spectra of bovine oxyhemoglobin, deoxyhemoglobin, carboxyhemoglobin, and methemoglobin," *Comp. Biochem. Physiol.* **118**(4), 743–749 (1997).
4. S. L. Jacques, R. D. Glickman, and J. A. Schwartz, "Internal absorption coefficient and threshold for pulsed laser disruption of melanosomes isolated from retinal pigment epithelium," *Proc. SPIE* **2681**, 468–477 (1996).
5. G. V. G. Baranoski et al. "On the noninvasive optical monitoring and differentiation of methemoglobinemia and sulfhemoglobinemia" *J. Biomed. Opt.* **17**(9), 097005 (2012).
6. S. Haymond et al, "Laboratory assessment of oxygenation in methemoglobinemia," *Clin. Chem.* **51**(2), 434–444 (2005).
7. R. K. Murray, D. K. Granner, and V. W. Rodwell, *Harper's Illustrated Biochemistry*, 27th ed., McGraw Hill Companies, Asia (2006).
8. M. C. Kohn et al., "Pharmacokinetics of sodium nitrite-induced methemoglobinemia in the rat," *Drug. Metab. Dispos.* **30**, 676–683 (2002).
9. S. S. Da-Silva, I. S. Sajan, and J. P. Underwood, "Congenital methemoglobinemia: a rare cause of cyanosis in the newborn—a case report," *Pediatrics* **112**, e158–e161 (2003).
10. R. B. May, "An infant with sepsis and methemoglobinemia," *J. Emerg. Med.* **3**, 261–264, (1985).
11. K. Ohashi et al., "Elevated methemoglobin in patients with sepsis," *Acta. Anaesthesiol. Scand.* **42**, 713–716, (1998).

12. R. O. Wright, W. J. Lewander, and A. D. Woolf, "Methemoglobinemia: etiology, pharmacology, and clinical management," *Ann. Emerg. Med.* **34**, 646–656 (1999).

13. World Health Organization, "Nitrate and nitrite in drinking-water," WHO/FWC/WSH/16.52 (2016).

14. G. F. Craun, D. G. Greathouse, and D. H. Gunderson. "Methemoglobin levels in young children consuming high nitrate well water in the United States," *Int. J. Epidem.* **10**, 309–317 (1981).

15. K. Kern, P. B. Langevin, and B. M. Dunn, "Methemoglobinemia after topical anesthesia with lidocaine and benzocaine for a difficult intubation," *J. Clin. Anesth.* **12**, 167–172 (2000).

16. R. K. Singh et al., "Benzocaine induced methemoglobinemia accompanying adult respiratory distress syndrome and sepsis syndrome: case report," *J. Trauma* **50**, 1153–1157 (2001).

17. C. Udeh, J. Bittikofer, and S. T. Sum-Ping, "Severe methemoglobinemia on reexposure to benzocaine," *J. Clin. Anesth.* **13**, 128–130 (2001).

18. H. U. Rehman, "Methemoglobinemia," *West. J. Med.* **175**(3), 193–196 (2001).

19. S. J. Barker, K. K. Tremper, and J. Hyatt, "Effects of methemoglobinemia on pulse oximetry and mixed venous oximetry," *Anesthesiology* **70**, 112–117 (1989).

20. C. M. Alexander, L. E. Teller, and J. B. Gross, "Principles of pulse oximetry: theoretical and practical considerations," *Anesth. Analg.* **68**, 368–376 (1989).

21. L. Delwood et al., "Methemoglobinemia and its effect on pulse oximetry," *Crit. Care. Med.* **19**, 988 (1991).

22. A. S. O. Tang et al., "The mystery of 'saturation gap': a case of dapsone-induced methaemoglobinemia in a pregnant mother with leprosy," *Oxf. Med. Case Rep.* **2019**(1), 8–10 (2019).

23. R. Ash-Bernal, R. Wise, and S. M. Wright, "Acquired methemoglobinemia: a retrospective series of 138 cases at 2 teaching hospitals," *Medicine* **83**(5), 265–273 (2004).

24. E. H. Annabi and S. J. Barker, "Severe methemoglobinemia detected by pulse oximetry," *Anesth. Analg.* **108**(3), 898–899 (2009).

25. J. R. Feiner and P. E. Bickler, "Improved accuracy of methemoglobin detection by pulse CO-oximetry during hypoxia," *Anesth. Analg.* **111**(5), 1160–1167 (2010).

26. N. Shah et al., "Performance of three new-generation pulse oximeters during motion and low perfusion in volunteers," *J. Clin. Anesth.* **24**(5), 385–391 (2012).

27. J. Lee et al., "Noninvasive *in vivo* monitoring of methemoglobin formation and reduction with broadband diffuse optical spectroscopy," *J. Appl. Physiol.* **100**(2), 615–622 (2006).

28. J. B. Fishkin et al., "Frequency-domain method for measuring spectral properties in multiple-scattering media: methemoglobin absorption spectrum in a tissuelike phantom," *Appl. Opt.* **34**, 1143–1155 (1995).

29. R. B. Saager et al., "Impact of hemoglobin breakdown products in the spectral analysis of burn wounds using spatial frequency domain spectroscopy," *J. Biomed. Opt.* **24**(2), 020501 (2019).

30. G. Leung et al., "Rapid tissue viability evaluation using methemoglobin as a biomarker in burns," *Int. J. Burns Trauma* **8**(5), 126–134 (2018).

31. M. Tang et al., "Noninvasive photoacoustic microscopy of methemoglobin *in vivo*," *J. Biomed. Opt.* **20**(3), 036007 (2015).

32. K. Aizawa et al., "*In vivo* photoacoustic spectroscopic imaging of hemoglobin derivatives in thermally damaged tissue," *Jpn. J. Appl. Phys.* **48**, 062302 (2009).

33. G. Zonios, J. Bykowski, and N. Kollias, "Skin melanin, hemoglobin, and light scattering properties can be quantitatively assessed *in vivo* using diffuse reflectance spectroscopy," *J. Invest. Dermatol.* **117**, 1452–1457 (2001).

34. S.-H. Tseng et al., "Chromophore concentrations, absorption and scattering properties of human skin *in vivo*," *Opt. Express* **17**, 14599–14617 (2009).

35. I. Nishidate, Y. Aizu, and H. Mishina, "Estimation of melanin and hemoglobin in skin tissue using multiple regression analysis aided by Monte Carlo simulation," *J. Biomed. Opt.* **9**(4), 700–710 (2004).

36. A. Nkengne et al., "'SpectraCam®: a new polarized hyperspectral imaging system for repeatable and reproducible *in vivo* skin quantification of melanin, total hemoglobin, and oxygen saturation," *Skin Res. Technol.* **24**, 99–107 (2018).

37. S. F. Bish et al., "Handheld diffuse reflectance spectral imaging (DRSi) for in-vivo characterization of skin," *Biomed. Opt. Express* **5**, 573–586 (2014).
38. B. S. Sorg et al., "Hyperspectral imaging of hemoglobin saturation in tumor microvasculature and tumor hypoxia development," *J. Biomed. Opt.* **10**(4), 044004 (2005).
39. I. Nishidate et al., "Non-invasive spectral imaging of skin chromophores based on multiple regression analysis aided by Monte Carlo simulation," *Opt. Lett.* **36**, 3239–3241 (2011).
40. M. Kohl et al., "Physical model for the spectroscopic analysis of cortical intrinsic optical signals," *Phys. Med. Biol.* **45**(12), 3749–3764 (2000).
41. P. B. Jones et al., "Simultaneous multispectral reflectance imaging and laser speckle flowmetry of cerebral blood flow and oxygen metabolism in focal cerebral ischemia," *J. Biomed. Opt.* **13**(4), 044007 (2008).
42. L. Wang, S. L. Jacques, and L. Zheng, "MCML: Monte Carlo modeling of light transport in multi-layered tissues," *Comput. Methods Prog. Biomed.* **47**, 131–146 (1995).
43. "FDA Drug Safety Communication: FDA continues to receive reports of a rare, but serious and potentially fatal adverse effect with the use of benzocaine sprays for medical procedures," 2011, https://www.fda.gov/drugs/drug-safety-and-availability/fda-drug-safety-communication-fda-continues-receive-reports-rare-serious-and-potentially-fatal
44. I. Nishidate et al., "Estimation of melanin and hemoglobin using spectral reflectance images reconstructed from a digital RGB image by the Wiener Estimation Method," *Sensors* **13**, 7902–7915 (2013).

Fahima Khatun received her DVM and MS degrees in parasitology from Bangladesh Agricultural University in 2010 and 2012, respectively. She is a PhD student at Tokyo University of Agriculture and Technology. Her current research interest is biomedical optics for disease diagnosis of human and animal beings.

Yoshihisa Aizu is a professor at Muroran Institute of Technology, Japan. He received his BE degree in electronics from Musashi Institute of Technology in 1980, ME and PhD degrees in electronics from Hokkaido University in 1982 and 1985, respectively. From 1992 to 1993, he was a visiting researcher in University Erlangen, Germany. His current research activities are in applications of optical imaging, spectroscopy, colorimetry, and laser speckle imaging to human and biological objects.

Izumi Nishidate received his MS and PhD degrees from Muroran Institute of Technology, Japan. He is an associate professor in the Graduate School of Bio-Applications and Systems Engineering, Tokyo University of Agriculture and Technology. His research interests include diffuse reflectance spectroscopy, light transport in biological tissues, multispectral imaging, *in vivo* functional imaging of living tissues, and photodynamic therapy.